Soil frost-enabled soil moisture precipitation feedback over northern high latitudes

Stefan Hagemann[1*], Tanja Blome[1], Altug Ekici[2] and Christian Beer[3]

[1] Max-Planck-Institut für Meteorologie, Bundesstr. 53, 20146 Hamburg, Deutschland,
[*] Tel.: +49 40 4117 3101, Email: stefan.hagemann@mpimet.mpg.de

[2] Earth System Sciences, Laver Building, University of Exeter, Exeter, UK

[3] Department of Environmental Science and Analytical Chemistry (ACES) and Bolin Centre for Climate Research, Stockholm University, Stockholm, Sweden.

Abstract

Permafrost or perennially frozen ground is an important part of the terrestrial cryosphere; roughly one quarter of Earth's land surface is underlain by permafrost. The currently observed global warming is most pronounced in the Arctic region and is projected to persist during the coming decades due to anthropogenic CO2 input. This warming will certainly have effects on the ecosystems of the vast permafrost areas of the high northern latitudes. The quantification of such effects, however, is still an open question. This is partly due to the complexity of the system, including several feedback mechanisms between land and atmosphere. In this study we contribute to increasing our understanding of such land-atmosphere interactions using an Earth system model (ESM) which includes a representation of cold region physical soil processes, especially the effects of freezing and thawing of soil water on thermal and hydrological states and processes. The coupled atmosphere-land models of the ESM of the Max Planck Institute for Meteorology, MPI-ESM, have been driven by prescribed observed SST and sea ice in an AMIP2-type setup with and without newly implemented cold region soil processes. Results show a large improvement in the simulated discharge. On one hand this is related to an improved snowmelt peak of runoff due to frozen soil in spring. On the other hand a subsequent reduction of soil moisture enables a positive feedback to precipitation over the high latitudes, which reduces the model's wet biases in precipitation and evapotranspiration during the summer. This is noteworthy as soil moisture – atmosphere feedbacks have previously not been in the research focus over the high latitudes. These results point out the importance of high latitude physical processes at the land surface for the regional climate.

Keywords: Soil moisture – precipitation feedback, soil water freezing, permafrost regions, global climate modelling, high latitudes

1 Introduction

Roughly one quarter of the northern hemisphere terrestrial land surface is underlain by permafrost (Brown et al., 1997; French, 1990), which is defined as ground that is at or below zero degrees Celsius for more than two consecutive years. Permafrost soils build a globally relevant carbon reservoir as they store large amounts of deep-frozen organic material with high carbon contents (Ping et al., 2008) leading to a total pan-Arctic estimate of 1300 Pg of soil carbon (C) in these areas (Hugelius et al., 2014), which is twice the amount of the atmosphere's content. Moreover, the high northern latitudes are one of the critical regions of anthropogenic climate change, where the observed warming is clearly above average due to the so-called Arctic Amplification (Solomon et al., 2007; ACIA, 2005). Climate model simulations project this trend to continue (Serreze and Barry, 2011). The combination of the high C stocks in sub-arctic and arctic soils with the pronounced warming in the affected regions could thus lead to a positive biogeochemical feedback through the release of formerly trapped, 'deep-frozen' C into the atmosphere, when near-surface permafrost thaws. For the thawed soils and their biogeochemistry, it is decisive whether dry or wet conditions predominate: Aerobic decomposition is relatively fast and leads to the release of CO2, while anaerobic decomposition is much slower and leads to the release of CH4 as the main product of the combustion of organic soil material. CH4 is a much more potent greenhouse gas, but has a shorter lifetime of about 10 years after which it is converted to CO2 by oxidation. Therefore, not only the soil's temperature, but also its moisture status are important for the assessment of the biogeochemical response to climatic conditions, and thus should be represented in climate or Earth System models in a realistic and process-based manner. Thus, the adequate representation of permafrost hydrology is a necessary and challenging task in Earth system modelling.

Hagemann et al. (2013a) described relevant hydrological processes that occur in permafrost areas and that should preferably be represented in models simulating interactions of permafrost hydrology with vegetation, climate and the carbon cycle. The current state of the representation of processes in general circulation models (GCMs) or Earth system models (ESMs) can be obtained by systematic model intercomparison through the various climate model intercomparison projects (CMIPs; Meehl et al., 2000) that have a long history within the climate modelling community. Results from CMIPs provide a good overview on the respective state of ESM model accuracy and performance. Koven et al. (2012) analysed the performance of ESMs from the most recent CMIP5 exercise over permafrost areas. They found that the CMIP5 models have a wide range of behaviours under the current climate, with many failing to agree with fundamental aspects of the observed soil thermal regime at high latitudes. This large variety of results originates from a substantial range in the level of complexity and advancement of permafrost-related processes implemented in the CMIP5 models (see, e.g., Hagemann et al., 2013a), whereas most of these models do not include permafrost specific processes, not even the most basic process of freezing and thawing of soil water. Due to missing processes and related deficiencies of their land surface schemes, climate models often show substantial biases in hydrological variables over high northern latitudes (Luo et al., 2003; Swenson et al., 2012). Moreover, the land surface parameterizations used in GCMs usually do not adequately resolve the soil conditions (Walsh et al., 2005). The parameterizations often rely on either point measurements or on information derived from satellite data. Therefore, large efforts are ongoing to extend ESMs in this respect, in order to improve simulated soil moisture profiles and associated ice contents, river discharge, surface and sub-surface runoff. The ESM improvement over permafrost areas was, e.g., one of the research objectives of the European Union Project PAGE21 (www.page21.org).

The most basic process in permafrost areas is the seasonal freezing and thawing of soil water in the presence of continuously frozen ground below a certain depth. The response of the soil to freezing leads to specific variations in the annual cycle of soil hydrology. Frozen ground and snow cover also influence rainfall-runoff partitioning, the timing and magnitude of spring runoff, and the amount of soil moisture that subsequently is available for evapotranspiration in spring and summer (Beer et al., 2006; Beer et al., 2007; Koren et al., 1999). Soil moisture controls the partitioning of the available energy into latent and sensible heat flux and conditions the amount of surface runoff. By controlling evapotranspiration, it is linking the energy, water and carbon fluxes (Koster et al., 2004; Dirmeyer et al., 2006; Seneviratne and Stöckli, 2008). Seneviratne et al. (2006) stated that a northward shift of climatic regimes in Europe due to climate change will result in a new transitional climate zone between dry and wet climates with strong land–atmosphere coupling in central and eastern Europe. They specifically highlight the importance of soil-moisture–temperature feedbacks (in addition to soil-moisture–precipitation feedbacks) for future climate changes over this region. A comprehensive review on soil moisture feedbacks is given by Seneviratne et al. (2010).

Largely, soil moisture feedbacks to the atmosphere are confined to regions where the evapotranspiration is moisture-limited. These are regions where the soil moisture is in the transitional regime between the permanent wilting point (soil moisture content below which the plants can not extract water from the soil by transpiration as the suction forces of the soil are larger than the transpiration forces of the plants) and the critical soil moisture W_{crit} above which plants transpire at the potential rate imposed by the atmospheric conditions, i.e. the potential evapotranspiration (see, e.g., Fig. 5 in Seneviratne et al., 2010). In this respect, the high-latitudes are usually excluded from those regions as they are considered to be predominantly energy-limited (Teuling et al., 2009), and where the coupling between soil moisture and the atmosphere does not play a role (Koster et al., 2004, 2006).

Note that in previous studies where an ESM's land surface model (LSM) was equipped with cold region soil processes, effects of resulting model improvements usually have not been directly considered in a coupled atmosphere-land context. Either simulated changes were only considered in the LSM standalone mode (e.g. Ekici et al., 2014, 2015; Lawrence and Slater, 2005; Gouttevin et al., 2012; Slater et al., 1998), or changes between different LSM version were not limited to cold region processes alone (Cox et al., 1999). Only Takata and Kimoto (2000) conducted a kind of precursor to our study who used a very coarse resolution atmospheric GCM (600 km resolution), but they neither used large-scale observations to evaluate the results of their study nor specifically addressed land-atmosphere feedbacks. Thus, soil moisture feedbacks to the atmosphere related to cold region soil processes have generally been neglected so far.

In the present study, we show that the implementation of cold region soil processes into the ESM of the Max Planck Institute for Meteorology, MPI-ESM, has a pronounced impact on the simulated terrestrial climate over the northern high latitudes, and that this is mainly related to a positive soil moisture-precipitation feedback. Section 2 introduces the used ESM version and the setup of the associated simulations, Section 3 discusses the main results over several high latitude river catchments, followed by a summary and conclusions in Section 4.

2 Model, data and methods

2.1 Model description

In this study, the atmosphere and land components of the ESM of the Max Planck Institute for Meteorology (MPI-M), MPI-ESM 1.1, are utilized that consist of the atmospheric GCM ECHAM6.3 (Stevens et al., 2013) and its land surface scheme JSBACH 3.0 (Raddatz et al., 2007, Brovkin et al., 2009). Both models have undergone several further developments since

132 the version (ECHAM6.1/JSBACH 2.0) used for the Coupled Model Intercomparison Project
133 5 (CMIP5; Taylor et al., 2012). Several bug fixes in the ECHAM physical parameterizations
134 led to energy conservation in the total parameterized physics and a re-calibration of the cloud
135 processes resulted in a medium range climate sensitivity of about 3 K. JSBACH 3.0
136 comprises several bug fixes, a new soil carbon model (Goll et al., 2015) and a five layer soil
137 hydrology scheme (Hagemann and Stacke, 2015) replaced the previous bucket scheme. These
138 five layers correspond directly to the structure used for soil temperatures and they are defined
139 with increasing thickness (0.065, 0.254, 0.913, 2.902, and 5.7 m) down to a lower boundary at
140 almost 10 m depth. In addition, a permafrost-ready version of JSBACH is considered
141 (JSBACH-PF) in which physical processes relevant at high latitude land regions have been
142 implemented by Ekici et al. (2014). Most importantly, these processes comprise the freezing
143 and thawing of soil moisture. Consequently, the latent heat of fusion dampens the amplitude
144 of soil temperature, infiltration is decreased when the uppermost soil layer is frozen, soil
145 moisture is bound in solid phase when frozen, and, hence, cannot be transported vertically or
146 horizontally. Dynamic soil thermal properties now depend on soil texture as well as on soil
147 water and ice contents. Dynamic soil hydraulic properties that depend on soil texture and soil
148 water content may decrease when soil moisture freezes (such as, e.g., the hydraulic
149 conductivity). Moreover a snow scheme has been implemented in which snow can develop in
150 up to five layers while the current scheme only represents up to two layers. In the original
151 snow scheme, the snow is thermally growing down inside the soil, i.e. the snow cover
152 becomes part of the soil temperature layers so that soil temperatures are mixed with snow
153 temperatures. In the new scheme, snow is accumulated on top of the soil using snow thermal
154 properties. Further, a homogeneous organic top layer is added with a constant depth and
155 specific thermal and hydraulic properties. Note that in the following the term soil moisture
156 generally refers to the liquid soil moisture if not mentioned otherwise. In this respect, total

157 soil moisture refers to the sum of liquid and frozen soil moisture.

158 ### 2.2 Experimental setup

159 Two ECHAM6.3/JSBACH simulations were conducted at T63 horizontal resolution (about
160 200 km) with 47 vertical layers in the atmosphere. They were forced by observed sea surface
161 temperature (SST) and sea ice from the AMIP2 (Atmospheric Model Intercomparison Project
162 2) dataset during 1970-2009 (Taylor et al., 2000). 1970-1988 are regarded as spin-up
163 phase,only the period 1989-2009 is considered for the analyses. The two simulations are:

164 • ECH6-REF: Simulation with the standard version of JSBACH 3.0 with a fixed
165 vegetation distribution and using a separate upper layer reservoir for bare soil
166 evaporation as described in Hagemann and Stacke (2015). Note that the latter is
167 switched off by default in JSBACH 3.0 to achieve a better performance of simulated
168 primary productivity, which is not of interest in the present study.
169 • ECH6-PF: As ECH6-REF, but using JSBACH-PF.

170 Note that both simulations used initial values of soil moisture, soil temperature and snowpack
171 that were obtained from an offline-simulation (land only) using JSBACH (as in ECH6-REF)
172 forced with WFDEI data (Weedon et al., 2014).

173 ### 2.3 Calculation of internal model climate variability

174 The internal climate variability of ECHAM6/JSBACH with respect to 20-year mean values
175 has been estimated from results of three 20-year, 5-member ensembles, in which the
176 ensembles used different land-atmosphere coupling setups (deVrese et al., 2016). Within each
177 ensemble, the model setup is identical but the simulations were started using slightly differing
178 initial conditions. Following the approach of Hagemann et al. (2009), we first calculated the

179 standard deviation of 20-year means for each ensemble, and then the spread for each model
180 grid box is defined as the maximum of the three ensemble standard deviations. This spread is
181 then used as an estimate of the model's internal climate variability. Thus, if simulated
182 differences between ECH6-PF and ECH6-REF are larger than this spread, they are considered
183 as robust and directly related to the introduction of cold region soil processes into JSBACH.

184 **2.4 Observational data**

185 We use climatological observed river discharges from the station network of the Global
186 Runoff Data Centre (Dümenil Gates et al., 2000). Near surface air (2m) temperature and
187 precipitation are taken from the recent global WATCH dataset of hydrological forcing data
188 (WFDEI; Weedon et al., 2014). The WFDEI combine the daily statistics of the Interim re-
189 analysis of the European Centre for Medium-Range Weather Forecasts (ERA-Interim; Dee et
190 al., 2011) with the monthly mean observed characteristics of temperature from the Climate
191 Research Unit dataset TS2.1 (CRU; Mitchell and Jones, 2005) and precipitation from the
192 Global Precipitation Climatology Centre full dataset version 4 (GPCC; Fuchs et al., 2007).
193 For the latter, a gauge-undercatch correction following Adam and Lettenmaier (2003) was
194 used, which takes into account the systematic underestimation of precipitation measurements
195 that have an error of up to 10-50% (see, e.g. Rudolf and Rubel, 2005).

196 For an estimate of observed evapotranspiration (ET), we are using data from the LandFlux-
197 EVAL dataset. This new product was generated to compile multi-year global merged
198 benchmark synthesis products based on the analyses of existing land evapotranspiration
199 datasets (monthly time scale, time periods 1989-1995 and 1989-2005). The calculation and
200 analyses of the products are described in Mueller et al. (2013). In our study we are using the
201 diagnostic products available for the period 1989-2005 that are based on various observations,
202 i.e. from remote sensing, diagnostic estimates (atmospheric water-balance estimates) and

ground observations (flux measurements). Here, we considered the mean, minimum and maximum of the respective diagnostic ensemble.

Surface solar irradiance (SSI; 2000-2010) is taken from the Clouds and Earth Radiation Energy System (CERES; Kato et al., 2013) that provides surface solar radiation fluxes at global scale derived from measurements onboard of the EOS Terra and Aqua satellites (Loeb et al., 2012). We used surface albedo data from MODIS (MCD43C3, ver5; 2000-2011; Cescatti et al., 2012), CERES (2000-2010) and the GlobAlbedo project (1998-2011; Muller et al., 2012) of the European Space Agency (ESA). With regard to the accumulated snowpack, we compared model data to snow water equivalent data from the ESA GlobSnow project (Takala et al., 2011), NASA's Modern-Era Retrospective Analysis for Research and Applications (MERRA; 1979-2013; Rienecker et al., 2011) and the snow data climatology (SDC) of Foster and Davy (1988).

3 Results

The simulations ECH6-REF and ECH6-PF are evaluated over the northern high latitudes analogously to how the evaluation of surface water and energy fluxes of the CMIP5 version of MPI-ESM was conducted by Hagemann et al. (2013b). The main differences in precipitation and 2m temperature between both simulations occur in the boreal summer. In ECH6-PF, precipitation is generally reduced compared to ECH6-REF over the northern high latitudes (Fig. 1). On the one hand, this leads to a general reduction of the wet bias compared to WFDEI data over the more continental areas north of about 60°N, especially over Canada and Russia. On the other hand, it enhances the dry bias over the adjacent mid-latitudes. Note that this summer dry bias of MPI-ESM 1.1 over mid-latitudes is more pronounced and wide-spread than in the CMIP5 version of MPI-ESM (cf. Fig. 4, middle row, in Hagemann et al.,

2013b), which is likely associated with bug-fixes or the re-calibration of cloud processes in ECHAM6.3 (cf. Sect. 2.1). The same is also the case for northern hemisphere summer warm biases in ECH6-REF (Fig. 2). These warm biases are enhanced in ECH6-PF. This enhancement is partly related to the fact that the reduced precipitation is accompanied by a reduced cloud cover, and, hence an increased incoming solar radiation at the land surface (Fig. 3). Compared to CERES data, the low bias in SSI over the high latitudes is largely removed while the overestimation over the mid-latitudes is slightly increased. The reason for the warmer air temperatures can partly be found in a decreased evapotranspiration (ET) when permafrost relevant physical soil processes are switched on. A detailed analysis of their effects was carried out to elucidate the specific influence of these processes and is shown for two large example catchments (Fig. 4). 1) The Arctic catchment is represented by the six largest rivers flowing into the Arctic Ocean: Kolyma, Lena, Mackenzie, Northern Dvina, Ob and Yenisei. The associated catchments comprise a large fraction of permafrost covered areas. 2) The Baltic Sea catchment includes only a low amount of permafrost covered areas but soil moisture freezing still plays a role over large parts of the catchment during the winter.

Arctic River catchments

ECH6-PF simulates the discharge of the six largest Arctic rivers more reliably than ECH6-REF, especially with regard to timing and size of the snow melt induced discharge peak in spring (Fig. 5a). This is largely related to the fact that in ECH6-PF, a major part of the snow melt turns into surface runoff as it cannot infiltrate into the ground when this is still frozen in the beginning of spring. This is opposite to ECH6-REF where larger parts of the snow melt are infiltrating into the soil due to the missing freezing processes such that the observed discharge peak is largely underestimated.

Consistent with Fig. 1, the large wet bias in the summer precipitation of ECH6-REF is

strongly reduced in ECH6-PF (Fig. 5c). This reduction in summer precipitation is accompanied by a reduction in summer evapotranspiration (Fig. 6a) that is now much closer to the mean of diagnostic estimates from the LandFlux dataset, while it is likely overestimated in ECH6-REF as the simulated evapotranspiration is close to the upper limit of the LandFlux diagnostic estimates. This ET reduction in ECH6-PF is directly related to a completely changed seasonal cycle of liquid relative soil moisture (actual soil moisture divided by the maximum soil water holding capacity) in the root zone (Fig. 6c). In ECH6-REF, the soil is very wet throughout the whole year with somewhat lower values in summer that are related to the summer ET. In ECH6-PF, the soil is rather dry in winter as larger parts of the total soil moisture are frozen (Fig. 7), and, hence, not accessible for ET. With infiltration of snowmelt in the spring when the soil water of the upper layer has thawed, the soil moisture is increasing and reaches its maximum in summer. The total amount of liquid soil moisture in ECH6-PF is much lower than in ECH6-REF. On the one hand large parts of the soil are frozen in winter and adjacent months (Fig. 7), and on the other hand this is related to the much lower infiltration in spring, so that less soil moisture is available throughout the whole year. In the autumn and winter, the amount of total soil moisture is somewhat increasing (Fig. 6c) as due to freezing, it is locally bound and can neither flow off laterally nor evaporate. If compared to the model's internal climate variability (Fig. 8) we note that the differences between ECH6-PF and ECH6-REF are robust for ET and precipitation from April-October and April-August, respectively.

The decreased ET during warm months, however, brings about less evaporative cooling of the land surface and a reduced upward moisture flux into the atmosphere that in turn seems to reduce cloud cover, and, hence SSI is increased in ECH6-PF (Fig. 9c, see also Fig. 3). Both of these effects result in a further increase of the summer warm bias in 2m air temperature (Fig. 9a, see also Fig. 2).

The surface albedo is rather similar in both experiments (Fig. 10a) but shows some distinct biases if compared to various observational datasets. During the winter JSBACH seems to overestimate the mainly snow-related albedo, indicating that it may have difficulties to adequately represent snow-masking effect of boreal forests [Note that a version of MODIS albedo data was used where low quality data over the very high northern latitudes were filtered out in the boreal winter due to too low available radiation (A. Löw, pers. comm., 2016). Due to these missing data over mainly snow covered areas, MODIS albedo averaged over the six largest Arctic rivers is biased low in the winter]. During the summer, there is a larger uncertainty in the observations. While the simulated albedo is close to MODIS and CERES data, it is lower than GlobAlbedo data. As a too low albedo would lead to a warm bias, this might indicate a better reliability of the GlobAlbedo data for this region in summer. Note that a sensitivity test where surface albedo was increased by 0.05 north of 60°N led to a reduction of the warm bias by about 1-2 K (not shown). As already indicated by the surface albedo, the simulated snow cover does not significantly differ between the experiments, either (Fig. 10c). It is lower than various observational estimates, which should impose a low albedo bias in winter. As this bias is in the opposite direction, it can be concluded that the low snow pack is compensating part of the snow masking problem mentioned above.

Baltic Sea catchment

A similar effect of the frozen ground is found over the Baltic Sea catchment, although this is less strong than for the Arctic rivers. The frozen ground leads to an enhanced snow melt runoff in spring (Fig. 5b) and a less strong replenishment of the ground by water during the winter as it is the case for ECH6-REF (Fig. 6d). Consequently the average level of liquid soil moisture is lower in ECH6-PF compared to ECH6-REF. This leads to more infiltration of water and less drainage, and hence, less runoff in the summer, which in turns leads to an

299 improved simulation of discharge (Fig. 5b). The impact on the atmosphere is much less
300 pronounced than for the Arctic rivers. On one hand there is less frozen ground in the Baltic
301 Sea catchment (Fig. 7), on the other hand the average soil moisture content is larger than for
302 the Arctic rivers (Fig. 6d). In ECH6-REF, the soil moisture is generally above W_{crit} (c.f. Sect.
303 1) in the Baltic Sea catchment so that ET is largely energy limited and mostly occurring at its
304 potential rate. Even though the ECH6-PF soil moisture is lower, it is generally still close to
305 W_{crit} so that ET is only slightly reduced, especially in the second half of the year (Fig. 6b).
306 Precipitation is also somewhat reduced (Fig. 5d) but this seems to be mostly related to the
307 internal climate variability except for September and October when a somewhat stronger and
308 robust reduction in ET leads to a robust precipitation decrease (Fig. 8).

309 # 4 Discussion and conclusions

310 The results described in the previous section show that soil freezing and thawing processes
311 enable the positive soil moisture-precipitation feedback (e.g. Dirmeyer et al., 2006;
312 Seneviratne et al., 2010) over large parts of northern mid- and high latitudes during the boreal
313 summer. The chain of processes leading to and influencing this feedback is sketched in Fig.
314 11. The frozen soil during the cold season (late autumn to early spring) leads to less
315 infiltration of rainfall and snowmelt during this season, and, hence, to more surface runoff
316 especially during the snowmelt period. On one hand this leads to a large improvement in
317 simulated discharge, mainly due to the improved snowmelt peak. This improved discharge
318 due to the representation of frozen ground has been also reported for other models (Beer et al.,
319 2006, 2007; Ekici et al., 2014; Gouttevin et al., 2012). On the other hand, this leads to a
320 decrease of soil moisture. This spring soil moisture deficit from the increased discharge
321 extents into the boreal summer due to the soil moisture memory (e.g. Koster and Suarez 2001,
322 Orth and Seneviratne 2012), when it actually causes more infiltration and less runoff, and,

hence, less discharge. The latter strongly improves the simulated discharge in the Baltic Sea catchment from summer to early winter. The decreased soil moisture leads to a reduced ET in regions where the soil moisture is in the transitional regime. Here, there is less recycling of moisture into the atmosphere, and the lower atmospheric moisture causes a reduction of precipitation that in turn leads to a further reduction of soil moisture.

Our new finding of the importance of the positive soil moisture-precipitation feedback in northern high latitudes has been supported by correlations between soil moisture and precipitation using monthly values from 1989-2009. While there are higher correlations between soil moisture and precipitation in the mid-latitudes for ECH6-REF (Fig. 12a), the high latitudes are mostly characterized by rather low correlations using the reference version of JSBACH. Figure 13b and c show that the correlation between soil moisture and precipitation is strongly increased in ECH6-PF over large parts of the northern high latitudes, especially over North America and eastern Siberia. This confirms an increased coupling of soil moisture and precipitation, and, hence, also indicates that the soil moisture-precipitation feedback is highly enabled in these areas. This positive soil moisture-precipitation feedback improves the simulated hydrological cycle, especially over the Arctic rivers where the wet biases in summer precipitation and ET are reduced. Less ET, and, hence, less evaporative cooling cause an increase in summer 2m air temperatures. This, in combination with more incoming surface solar radiation due to fewer clouds, increases and extends the existing summer warm bias of MPI-ESM north of about 50°N. Since air temperature is a main driver of soil freezing and thawing processes, there are more indirect interactions between energy and water balances which call for even more advanced factorial model experiments in the future.

Changes in the simulated hydrological cycle induced by the utilization of the improved soil

scheme are mostly confined to areas where freezing and thawing of water play a role. To illustrate this, Fig. 13 shows the number of months where in the climatological average of 1989-2009, the upper soil layer is below 0°C in ECH6-PF. Changes in precipitation (Fig. 1) and surface solar irradiance (Fig. 3), indicating changes in cloud cover, are mostly located in regions where the upper layer is frozen for at least three months within the climatological average. Changes outside of regions with soil frost may be imposed by changed atmospheric humidity and heat transport from soil frost affected regions on the one hand. On the other hand, Ekici et al. (2014) also introduced a permanent, static organic top layer as part of the new JSBACH-PF soil scheme. If switched on, as in the current ECH6-PF simulation, it is considered globally uniform, thus introducing a soil isolating effect also outside permafrost regions. As a consequence, the partitioning of the surface heat balance is altered during snow-free months towards a decreased ground heat flux, which needs to be compensated for by the turbulent heat fluxes, in particular by the sensible heat flux. This in turn contributes to the warming of the 2m air temperature which can be seen also in areas without any soil frost (Fig. 2). Even though the uniform organic insulation layer was implemented globally, Fig. 12 shows that the correlation between soil moisture and precipitation advances strongly in northern high latitudes only while this correlation has nearly not changed in the temperate zone and in particular in drought-dominated areas in south-east Europe or mid-west USA. Note that currently, the land surface scheme has been further advanced by a mechanistic model of mosses and lichens dynamics (Porada et al., 2016) which will replace the actual static organic top layer for soil insulation. This will enable a more realistic representation of the temporal and spatial variation of the soil insulation.

A positive soil moisture-precipitation feedback has not been pointed out for the northern high latitudes so far, even though in their coarse resolution GCM study, Takata and Kimoto (2000) found similar impacts to those shown in Fig. 11 induced by soil water freezing. Previously,

372 the northern high latitudes have generally been considered as energy-limited regimes where
373 land-atmosphere coupling due to soil moisture does not play a role (e.g. Teuling et al., 2009).
374 But this principal feedback loop has been found for drier regions where the soil moisture is
375 generally in the transitional regime and land-atmosphere coupling plays a role. Koster et al.
376 (2004) considered the strength of coupling between soil moisture and precipitation in an
377 ensemble of atmospheric GCMs. The resulting map is very similar to the map regarding the
378 strength of coupling between soil moisture and temperature in the same GCMs (Koster et al.,
379 2006). This suggests that in these models, the same process controls both couplings, namely
380 the ET sensitivity to soil moisture that leads to a positive feedback (Seneviratne et al., 2010).
381 But on the one hand it can be assumed that many models participating in those earlier studies
382 did not include the freezing and thawing of soil water. Thus, our reference simulation ECH6-
383 REF is in line with results reported in the literature, generally not showing a strong coupling
384 between precipitation and soil moisture in permafrost regions, such as indicated by the rather
385 low correlation values in Fig. 12a. Only the ECH6-PF simulation using advanced soil physics
386 shows that such strong coupling indeed is present (Fig. 12b). On the other hand, only annual
387 mean diagnostics were considered in some of those earlier studies (e.g. Teuling et al., 2009).
388 In other land-atmosphere coupling studies, that, e.g., followed the GLACE protocol such as
389 Koster et al. (2004), prescribed soil moisture conditions were used that were similar to the
390 average soil moisture climatology. Here, it seems that the differences between the simulations
391 with free and prescribed soil moisture in GLACE type simulations may be not large enough to
392 reveal a large-scale feedback over the high latitudes. This may only be possible by an
393 experimental design where more pronounced summer soil moisture changes are introduced.
394 Note that in the present study, these pronounced changes were introduced not due to an
395 artificial design, but they were caused by the implementation of previously missing frozen
396 soil physics into the model. Our study has shown that spring moisture deficits can lead to soil

moisture conditions during the boreal summer that allow for an advanced land-atmosphere coupling and a positive soil moisture-precipitation feedback over the northern high latitudes.

Even though our results are obtained with a modelling study, their physical consistency suggests that cold region soil processes, especially freezing and thawing of soil water, may lead to a positive soil moisture precipitation feedback during the summer in reality, too. A prerequisite for the occurrence of a soil moisture precipitation feedback is that soil moisture is in the transitional regime. Thus, the strength of the feedback depends on the wetness of the soil and, hence, is likely model dependent. Models with wetter/drier soils over the considered regions may simulate a weaker/stronger feedback.

Several modelling studies pointed out that there are not only positive feedback loops between soil moisture and precipitation but also negative ones that, under specific conditions, such as convective instability and/or cloud formation, may be stronger over dry soils (e.g. Hohenegger et al., 2009; Froidevaux et al., 2014). However, to date, the latter results appear mostly confined to single-column, cloud-resolving, and some high-resolution regional climate simulations (Seneviratne et al., 2010) and may also depend on the choice of the convective parameterisations (e.g. Giorgi et al., 1996). Guillod et al. (2015) noted that precipitation events tend to be located over drier patches, but they generally need to be surrounded by wet conditions; positive temporal soil moisture-precipitation relationships are thus driven by large-scale soil moisture. Thus, negative feedbacks seem to have more an impact on high resolution and thus on the local scale (Ho-Hagemann et al., 2015), where the effects of land surface heterogeneity for the inferred feedbacks also need to be taken into account (Chen and Avissar, 1994; Pielke et al., 1998; Taylor et al., 2013). Consequently most GCMs may not be able to represent negative feedbacks between soil moisture and precipitation via ET. As in the present study, we considered the effect of large-scale soil moisture changes due to soil

421 freezing processes, the identification of potential negative feedbacks on the local scale is
422 beyond the scope of the present study.

423 In MPI-ESM, an unwelcome effect of implementing cold region soil processes is the increase
424 of the existing warm bias over the high latitudes during summer. In order to estimate the
425 contribution of biases in SSI and surface albedo to this warm bias, we calculated an upper
426 limit for the temperature change that may be imposed by a radiation difference in the related
427 energy flux into the ground [SSI × (1 – albedo)]. For this estimation we assume that the
428 surface temperature is adjusting in a way that this radiation difference is compensated by
429 thermal radiation following the Stefan Boltzmann law. Here, any change in the turbulent
430 surface heat fluxes is neglected so that the resulting temperature change is an upper limit for
431 the temperature bias that might be explained by a radiation bias.

432 Considering the mean summer biases over the six largest Arctic rivers (Table 1) indicates that
433 a part of the warm bias may be attributed to the overestimation in SSI. For ECH6-PF (ECH6-
434 REF), the SSI bias may cause a warm bias of up to 2.9 K (0.9 K). The surface albedo may
435 contribute another 0.7 K (0.8 K) to the warm bias if compared to GlobAlbedo data but this is
436 a rather vague estimation due to the large uncertainty on surface albedo observations (see Fig.
437 10). Nevertheless biases in both of these variables cannot explain the full bias of 5 K (2.1 K)
438 in 2m temperature. Further contributions to this warm bias might be related to a too weak
439 vertical mixing of heat within the boundary layer or too much advection of warm air. The
440 latter may also influence the recycling ratio of water within and outside regions of soil frost.
441 A deeper investigation of this is beyond the scope of the present study and should be dealt
442 with in future model improvements.

443 We have shown that soil physical processes such as thawing and freezing have an impact on
444 the regional climate over the high latitude permafrost areas. Flato et al. (2013) reported that

CMIP5 GCMs tend to overestimate precipitation over northern high latitudes except for Europe and western Siberia. As many of these GCMs are still missing basic cold region processes, a missing interaction between soil moisture and precipitation in those GCMs is likely to contribute to this wet bias. An adequate implementation of physical soil processes into an ESM is only the first necessary step to yield an adequate representation of land-atmosphere interactions over the high latitudes. This also includes the incorporation of wetland dynamics, which will be the next step in the JSBACH development with regard to high latitudes, thereby following an approach of Stacke and Hagemann (2012). In addition, a reliable hydrological scheme for permafrost regions will allow investigations of related climate-carbon cycle feedback mechanisms (McGuire et al., 2006; Beer, 2008; Heimann and Reichstein, 2008).

Our findings demonstrate that soil freezing and thawing induce a much stronger coupling of land and atmosphere in northern high latitudes than previously thought. The additional importance of the positive soil moisture precipitation feedback in high latitudes will have a strong impact on future climate projections in addition to other biophysical (e.g. albedo) or biogeochemical (e.g. climate-carbon cycle) feedback mechanisms. Therefore, the findings of this study additionally highlight the importance of permafrost ecosystem functions in relation to climate.

Acknowledgments

The authors acknowledge the financial support of T. Blome by the European Union FP7-ENV project PAGE21 under contract number GA282700. S. Hagemann is supported by funding from the European Union within the Horizon 2020 project CRESCENDO (grant no. 641816).

References

468 ACIA: Arctic Climate Impact Assessment, Cambridge University Press, 1042p.,
469 http://www.acia.uaf.edu, 2005.

470 Adam, J. C., and, Lettenmaier, D. P.: Adjustment of global gridded precipitation for
471 systematic bias, J. Geophys. Res., 108, D9, 4257, doi:10.1029/2002JD002499, 2003.

472 Beer, C.: Soil science: The Arctic carbon count, Nature Geoscience, 1, 569-570,
473 doi:10.1038/ngeo292, 2008.

474 Beer, C., Lucht, W., Schmullius, C., and Shvidenko, A.: Small net carbon dioxide uptake by
475 Russian forests during 1981–1999, Geophys. Res. Lett., 33, L15403,
476 doi:10.1029/2006GL026919, 2006.

477 Beer, C., Lucht, W., Gerten, D., Thonicke, K., and Schmullius, C.: Effects of soil freezing and
478 thawing on vegetation carbon density in Siberia: A modeling analysis with the Lund-
479 Potsdam-Jena Dynamic Global Vegetation Model (LPJ-DGVM), Global Biogeochem.
480 Cyc., 21, GB1012, doi:10.1029/2006GB002760, 2007.

481 Brovkin, V., Raddatz, T., Reick, C. H., Claussen, M., and Gayler, V.: Global biogeophysical
482 interactions between forest and climate, Geophys. Res. Letters, 36, L07 405,
483 doi:10.1029/2009GL037543, 2009.

484 Brown, J., Ferrians Jr., O. J., Heginbottom, J. A., and Melnikov, E. S. (eds.): Circum-Arctic
485 map of permafrost and ground-ice conditions, Washington, DC: U.S. Geological Survey
486 in Cooperation with the Circum-Pacific Council for Energy and Mineral Resources.
487 Circum-Pacific Map Series CP-45, scale 1:10,000,000, 1997.

488 Cescatti, A., Marcolla, B., Santhana Vannan, S. K., Pan, J. Y., Román, M. O., Yang, X.,
489 Ciais, P., Cook, R. B., Law, B. E., Matteucci, G., Migliavacca, M., Moors, E.,
490 Richardson, A. D., Seufert, G., and Schaaf, C.B.: Intercomparison of MODIS albedo
491 retrievals and in situ measurements across the global FLUXNET network, Rem. Sens.

Environ., 121, 323-334, 2012.

Chen, F., and Avissar, R.: Impact of land-surface moisture variability on local shallow convective cumulus and precipitation in large-scale models, J. Appl. Meteorol., 33 (12), 1382–1401, 1994.

Cox, P., Betts, R., Bunton, C., Essery, R., Rowntree, P., and Smith, J.: The impact of new land surface physics on the GCM simulation. of climate and climate sensitivity, Climate Dyn., 15, 183–203, doi:10.1007/s003820050276, 1999.

de Vrese, P., and Hagemann, S.: Explicit representation of spatial sub-grid scale heterogeneity in an ESM, J. Hydrometeorol., 17, 1357-1371, doi:10.1175/JHM-D-15-0080.1., 2016.

Dee, D. P., Uppala, S. M., Simmons, A. J., Berrisford, P., Poli, P., Kobayashi, S., Andrae, U., Balmaseda, M. A., Balsamo, G., Bauer, P., Bechtold, P., Beljaars, A. C. M., van de Berg, L., Bidlot, J., Bormann, N., Delsol, C., Dragani, R., Fuentes, M., Geer, A. J., Haimberger, L., Healy, S. B., Hersbach, H., Hólm, E. V., Isaksen, L., Kållberg, P., Köhler, M., Matricardi, M., McNally, A. P., Monge-Sanz, B. M., Morcrette, J.-J., Park, B.-K., Peubey, C., de Rosnay, P., Tavolato, C., Th´epaut, J.-N., and Vitart, F.: The ERA-interim reanalysis: configuration and performance of the data assimilation system, Q. J. Roy. Meteorol. Soc., 137, 553–597, doi:10.1002/qj.828, 2011.

Dirmeyer, P., Koster, R., and Guo, Z. A. D.: Do global models properly represent the feedback between land and atmosphere?, J. Hydrometeorol., 7, 1177–1198, 2006.

Dümenil Gates, L., Hagemann, S., and Golz, C.: Observed historical discharge data from major rivers for climate model validation, Max Planck Institute for Meteor. Rep., 307 [available from MPI for Meteorology, Bundesstr. 53, 20146 Hamburg, Germany], 2000.

Ekici, A., Beer, C., Hagemann, S., Boike, J., Langer, M., and Hauck, C.: Simulating high latitude permafrost regions by the JSBACH terrestrial ecosystem model, Geosci. Model

516 Dev., 7, 631-647, doi:10.5194/gmd-7-631-2014, 2014.

517 Ekici, A., Chadburn, S., Chaudhary, N., Hajdu, L. H., Marmy, A., Peng, S., Boike, J., Burke,
518 E., Friend, A. D., Hauck, C., Krinner, G., Langer, M., Miller, P. A., and Beer, C.: Site-
519 level model intercomparison of high latitude and high altitude soil thermal dynamics in
520 tundra and barren landscapes, The Cryosphere, 9, 1343-1361, doi:10.5194/tc-9-1343-
521 2015, 2015.

522 Flato, G., Marotzke, J., Abiodun, B., Braconnot, P., Chou, S. C., Collins, W., Cox, P.,
523 Driouech, F., Emori, S., Eyring, V., Forest, C., Gleckler, P., Guilyardi, E., Jakob, C.,
524 Kattsov, V., Reason, C., and Rummukainen, M.: Evaluation of Climate Models. In:
525 Climate Change 2013: The Physical Science Basis, Contribution of Working Group I to
526 the Fifth Assessment Report of the Intergovernmental Panel on Climate Change [Stocker,
527 T.F., Qin, D., Plattner, G.-K., Tignor, M., Allen, S. K., Boschung, J., Nauels, A., Xia, Y.,
528 Bex, V., and Midgley, P. M. (eds.)]. Cambridge University Press, Cambridge, United
529 Kingdom and New York, NY, USA, 2013.

530 Foster, D. J., and Davy, R.D.: Global snow data climatology, USAFETAC/TN-88/006, Scott
531 Air Force Base III, 1988.

532 French, H. M.: Editorial, Permafrost Periglac. Process, 1, 1, doi: 10.1002/ppp.3430010102,
533 1990.

534 Froidevaux, P., Schlemmer, L., Schmidli, J., Langhans, W., and Schär, C.: Influence of
535 background wind on the local soil moisture-precipitation feedback, J. Atmos. Sci., 71,
536 782-799, 2014.

537 Fuchs, T., Schneider, U., and Rudolf, B.: Global Precipitation Analysis Products of the
538 GPCC, Global Precipitation Climatology Centre (GPCC). Deutscher Wetterdienst,
539 Offenbach, Germany, 2007.

Giorgi, F., Mearns, L.O., Shields, C., and Mayer, L.: A regional model study of the importance of local versus remote controls of the 1988 drought and the 1993 flood over the central United States, J. Climate, 9, 1150–1162, 1996.

Goll, D. S., Brovkin, V., Liski, J., Raddatz, T., Thum, T., and Todd-Brown, K. E. O.: Strong dependence of CO2 emissions from anthropogenic land cover change on initial land cover and soil carbon parametrization, Global Biogeochem. Cycles, 29, 1511–1523, doi:10.1002/2014GB004988, 2015.

Gouttevin, I., Krinner, G., Ciais, P., Polcher, J., and Legout, C.: Multi-scale validation of a new soil freezing scheme for a land-surface model with physically-based hydrology, The Cryosphere, 6, 407-430, doi:10.5194/tc-6-407-2012, 2012.

Guillod, B. P., Orlowsky, B., Miralles, D. G., Teuling, A. J., and Seneviratne, S. I.: Reconciling spatial and temporal soil moisture effects on afternoon rainfall, Nat. Commun., 6, 6443, doi: 10.1038/ncomms7443, 2015.

Hagemann, S., Göttel, H., Jacob, D., Lorenz, P., and Roeckner, E.: Improved regional scale processes reflected in projected hydrological changes over large European catchments, Climate Dyn., 32, 767-781, doi: 10.1007/s00382-008-0403-9, 2009.

Hagemann, S., Blome, T., Saeed, F., and Stacke, T.: Perspectives in modelling climate-hydrology interactions, Surveys in Geophys., 35, 739-764, ISSI special issue on Hydrological Cycle, doi:10.1007/s10712-013-9245-z, 2013a.

Hagemann, S., Loew, A., Andersson, A.: Combined evaluation of MPI-ESM land surface water and energy fluxes, J. Adv. Model. Earth Syst., 5, doi:10.1029/2012MS000173, 2013b.

Hagemann, S., and Stacke, T.: Impact of the soil hydrology scheme on simulated soil moisture memory, Climate Dyn., 44, 1731-1750, doi:10.1007/s00382-014-2221-6, 2015.

564 Heimann, M., and Reichstein, M.: Terrestrial ecosystem carbon dynamics and climate
565 feedbacks, Nature, 451, 289-292, 2008.

566 Ho-Hagemann, H. T. M., Rockel, B., and Hagemann, S.: On the role of soil moisture in the
567 generation of heavy rainfall during the Oder flood event in July 1997, Tellus A, 67,
568 28661, dx.doi.org/10.3402/tellusa.v67.28661, 2015.

569 Hohenegger, C., Brockhaus, P., Bretherton, C. S., and Schär, C.: The Soil Moisture–
570 Precipitation Feedback in Simulations with Explicit and Parameterized Convection, J.
571 Climate, 22, 5003–5020, 2009.

572 Hugelius, G., Strauss, J., Zubrzycki, S., Harden, J. W., Schuur, E. A. G., Ping, C.-L.,
573 Schirrmeister, L., Grosse, G., Michaelson, G. J., Koven, C. D., O'Donnell, J. A.,
574 Elberling, B., Mishra, U., Camill, P., Yu, Z., Palmtag, J., and Kuhry, P.: Estimated stocks
575 of circumpolar permafrost carbon with quantified uncertainty ranges and identified data
576 gaps, Biogeosciences, 11, 6573-6593, doi:10.5194/bg-11-6573-2014, 2014.

577 Kato, S., Loeb, N. G., Rose, F. G., Doelling, D. R., Rutan, D. A., Caldwell, T. E., Yu, L., and
578 Weller, R. A.: Surface irradiances consistent with CERES-derived top-of-atmosphere
579 shortwave and longwave irradiances, J. Climate, 26, 2719-2740, doi: 10.1175/JCLI-D-12-
580 00436.1, 2013.

581 Koren, V., Schaake, J., Mitchell, K., Duan, O. Y., Chen, F., and Baker, J. M.: A
582 parameterization of snowpack and frozen ground intended for NCEP weather and climate
583 models, J. Geophys. Res., 104, 19569–19585, 1999.

584 Koster, R. D., and Suarez, M. J.: Soil moisture memory in climate models. J. Hydrometeorol.,
585 2, 558-570, 2001.

586 Koster, R. D., Dirmeyer, P. A., Guo, Z., Bonan, G., Chan, E., Cox, P., Gordon, C. T., Kanae,
587 S., Kowalczyk, E., Lawrence, D., Liu, P., Lu, C. H., Malyshev, S., McAvaney, B.,

588 Mitchell, K., Mocko, D., Oki, T., Oleson, K., Pitman, A., Sud, Y. C., Taylor, C. M.,
589 Verseghy, D., Vasic, R., Xue, Y., and Yamada, T.: Regions of strong coupling between
590 soil moisture and precipitation, Science, 305, 1138–1140, 2004.

591 Koster R. D., Guo, Z., Dirmeyer, P. A., Bonan,, G., Chan, E., Cox, P., Davies, H., Gordon, C.
592 T., Kanae, S., Kowalczyk, E., Lawrence, D., Liu, P., Lu, C. H., Malyshev, S., McAvaney,
593 B., Mitchell, K., Mocko, D., Oki, T., Oleson, K. W., Pitman, A., Sud, Y. C., Taylor, C.
594 M., Verseghy, D., Vasic, R., Xue, Y., and Yamada, T.: GLACE: The Global Land-
595 Atmosphere Coupling Experiment. Part I: Overview, J. Hydrometeorol., 7, 590–610,
596 2006.

597 Koven, C. D., Riley, W. J., and Stern, A.: Analysis of permafrost thermal dynamics and
598 response to climate change in the CMIP5 Earth System Models, J. Climate, 26, 1877-
599 1900, doi:10.1175/JCLI-D-12-00228.1, 2012.

600 Lawrence, D. M., and Slater, A. G.: A projection of severe near-surface permafrost
601 degradation during the 21st century, Geophys. Res. Lett., 32, L24401,
602 doi:10.1029/2005GL025080, 2005.

603 Loeb, N. G., Kato, S., Su, W., Wong, T., Rose, F. G., Doelling, D. R., and Norris, J.:
604 Advances in understanding top-of-atmosphere radiation variability from satellite
605 observations, Surveys in Geophysics, doi: 10.1007/s10712-012-9175-1, 2012.

606 Luo, L. F., Robock, A., Vinnikov, K. Y., Schlosser, C. A., Slater, A. G., Boone, A., Braden,
607 H., Cox, P., de Rosnay, P., Dickinson, R. E., Dai, Y. J., Duan, Q. Y., Etchevers, P.,
608 Henderson-Sellers, A., Gedney, N., Gusev, Y. M., Habets, F., Kim, J. W., Kowalczyk, E.,
609 Mitchell, K., Nasonova, O. N., Noilhan, J., Pitman, A. J., Schaake, J., Shmakin, A. B.,
610 Smirnova, T. G., Wetzel, P., Xue, Y. K., Yang, Z. L., and Zeng, Q. C.: Effects of frozen
611 soil on soil temperature, spring infiltration, and runoff: Results from the PILPS 2(d)

612 experiment at Valdai, Russia, J. Hydrometeorol., 4, 334–351, 2003.

613 McGuire, A.D., Chapin III, F.S., Walsh, J.E. and Wirth, C.: Integrated regional changes in
614 arctic climate feedbacks: Implications for the global climate system, Annu. Rev. Environ.
615 Resour. 31, 61–91, doi:10.1146/annurev.energy.31.020105.100253, 2006.

616 Meehl, G. A., Boer, G. J., Covey, C., Latif, M., and Stouffer, R. J.: The Coupled Model
617 Intercomparison Project (CMIP), Bull. Amer. Meteor. Soc., 81, 313–318, 2000.

618 Mitchell, T. D., and Jones, P. D.: An improved method of constructing a database of monthly
619 climate observations and associated high-resolution grids, Int. J. Climatol., 25, 693-712,
620 2005.

621 Mueller, B., Hirschi, M., Jimenez, C., Ciais, P., Dirmeyer, P. A., Dolman, A. J., Fisher, J. B.,
622 Jung, M., Ludwig, F., Maignan, F., Miralles, D., McCabe, M. F., Reichstein, M.,
623 Sheffield, J., Wang, K. C., Wood, E. F., Zhang, Y., and Seneviratne, S. I.: Benchmark
624 products for land evapotranspiration: LandFlux-EVAL multi-dataset synthesis, Hydrol.
625 Earth Syst. Sci., 17, 3707-3720, doi:10.5194/hess-17-3707-2013, 2013.

626 Muller, J.-P., López, G., Watson, G., Shane, N., Kennedy, T., Yuen, P., Lewis, P., Fischer, J.,
627 Guanter, L., Domench, C., Preusker, R., North, P., Heckel, A., Danne, O., Krämer, U.,
628 Zühlke, M., Brockmann, C., and Pinnock, S.: The ESA GlobAlbedo Project for mapping
629 the Earth's land surface albedo for 15 Years from European Sensors., paper presented at
630 IEEE Geoscience and Remote Sensing Symposium (IGARSS) 2012, IEEE, Munich,
631 Germany, 22-27.7.12, 2012.

632 Orth, R., and Seneviratne, S.I.: Analysis of soil moisture memory from observations in
633 Europe. J. Geophys. Res. - Atmospheres, 117, D15115, 2012.

634 Pielke, R.A., Avissar, R., Raupach, M., Dolman, A.J., Zeng, X.B., and Denning, A.S.:
635 Interactions between the atmosphere and terrestrial ecosystems: influence on weather and

636 climate, Glob. Chang. Biol. 4 (5), 461–475, 1998.

637 Ping, C.L., Michaelson, G.J., Jorgenson, M.T., Kimble, J.M., Epstein, H., Romanovsky,
638 V.E., and Walker, D.A.: High stocks of soil organic carbon in the North American Arctic
639 region, Nat. Geosci., 1, 615-619, 2008.

640 Porada, P., Ekici, A., and Beer, C.: Effects of bryophyte and lichen cover on permafrost soil
641 temperature at large scale, The Cryosphere Discuss., doi:10.5194/tc-2015-223, in review,
642 2016.

643 Raddatz, T. J., Reick, C., Knorr, W., Kattge, J., Roeckner, E., Schnur, R., Schnitzler, K.-G.,
644 Wetzel, P., and Jungclaus, J. H.: Will the tropical land biosphere dominate the climate-
645 carbon cycle feedback during the twenty-first century?, Climate Dyn., doi:
646 10.1007/s00382-007-0247-8, 2007.

647 Rienecker, M. M., Suarez, M. J., Gelaro, R., Todling, R., Bacmeister, J., Liu, E., Bosilovich,
648 M. G., Schubert, S. D., Takacs, L., Kim, G.-K., Bloom, S., Chen, J., Collins, D., Conaty,
649 A., da Silva, A., Gu, W., Joiner, J., Koster, R. D., Lucchesi, R., Molod, A., Owens, T.,
650 Pawson, S., Pegion, P., Redder, C. R., Reichle, R., Robertson, F. R., Ruddick, A. G.,
651 Sienkiewicz, M., and Woollen, J: MERRA - NASA's Modern-Era Retrospective Analysis
652 for Research and Applications, J. Climate, 24, 3624-3648, doi:10.1175/JCLI-D-11-
653 00015.1, 2011.

654 Rudolf, B., and Rubel, F.: Global precipitation, In: Hantel. M. (ed): Observed global climate,
655 Chap. 11. Landolt–Boernstein: numerical data and functional relationships in science and
656 technology – new series, Group 5: Geophysics, vol. 6, Springer, Berlin Heidelberg New
657 York, p 567, 2005.

658 Seneviratne, S. I., and Stöckli, R.: The role of land-atmosphere interactions for climate
659 variability in Europe, In: Climate Variability and Extremes during the Past 100 years,

660 Brönnimann et al. (eds.), Adv. Global. Change. Res., 33, Springer Verlag. (Book chapter),
661 2008.

662 Seneviratne, S. I., Lüthi, D., Litschi, M., and Schär, C.: Land-atmosphere coupling and
663 climate change in Europe, Nature, 443, 205-209, 2006.

664 Seneviratne, S. I., Corti, T., Davin, E., Hirschi, M., Jaeger, E. B., Lehner, I., Orlowsky, B.,
665 and Teuling, A. J.: Investigating soil moisture-climate interactions in a changing climate:
666 A review, Earth-Sci. Rev., 99, 125-161, doi:10.1016/j.earscirev.2010.02.004, 2010.

667 Serreze, M. C., and Barry, R. G.: Processes and impacts of Arctic amplification: A research
668 synthesis, Global Planet Change, 77, 85-96, doi:10.1016/j.gloplacha.2011.03.004, 2011.

669 Slater, A., Pitman, A., and Desborough, C.: Simulation of freeze thaw cycles in a general
670 circulation model land surface scheme, J. Geophys. Res., 103, 11303–1131, 1998.

671 Solomon, S., Qin, D., Manning, M., Marquis, M., Averyt, K., Tignor, M. M. B., Miller Jr., H.
672 L., and Chen, Z. (Eds.): Climate change 2007: The physical science basis, Cambridge
673 University Press, 996 pp., 2007.

674 Stacke, T., and Hagemann, S.: Development and validation of a global dynamical wetlands
675 extent scheme, Hydrol. Earth Syst. Sci., 16, 2915-2933, doi:10.5194/hess-16-2915-2012,
676 2012.

677 Stevens, B., Giorgetta, M., Esch, M., Mauritsen, T., Crueger, T., Rast, S., Salzmann, M.,
678 Schmidt, H., Bader, J., Block, K., Brokopf, R., Fast, I., Kinne, S., Kornblueh, L.,
679 Lohmann, U., Pincus, R., Reichler, T., and Roeckner, E.: The atmospheric component of
680 the MPI-M Earth System Model: ECHAM6, J. Adv. Model Earth Syst., 5, 146-172.
681 doi:10.1002/jame.20015, 2013.

682 Swenson, S. C., Lawrence, D. M., and Lee, H.: Improved simulation of the terrestrial
683 hydrological cycle in permafrost regions by the Community Land Model, J. Adv. in

684 Modelling Earth Systems, 4, doi:10.1029/2012MS000165, 2012.

685 Takala, M., Luojus, K., Pulliainen, J., Derksen, C., Lemmetyinen, J., Kärnä, J.-P, Koskinen,
686 J., and Bojkov, B.: Estimating northern hemisphere snow water equivalent for climate
687 research through assimilation of spaceborne radiometer data and ground-based
688 measurements, Rem. Sens. Environ., 115, doi: 10.1016/j.rse.2011.08.014, 2011.

689 Takata, K., and Kimoto, M.: A numerical study on the impact of soil freezing on the
690 continental-scale seasonal cycle, J. Meteor. Soc. Japan, 78, 199-221, 2000.

691 Taylor, C. M., Birch, C. E., Parker, D. J., Dixon, N., Guichard, F., Nikulin, G., and Lister, G.
692 M. S.: Modeling soil moisture-precipitation feedback in the Sahel: Importance of spatial
693 scale versus convective parameterization, Geophys. Res. Lett., 40, 6213–6218,
694 doi:10.1002/2013GL058511, 2013.

695 Taylor, K. E., Williamson, D., and Zwiers, F.: The sea surface temperature and sea-ice
696 concentration boundary conditions for AMIP II simulations, PCMDI Report, 60, Program
697 for Climate Model Diagnosis and Intercomparison. Lawrence Livermore National
698 Laboratory, Livermore, California, 25 pp., 2000.

699 Taylor, K. E., Stouffer, R. J., and Meehl, G. A.: An overview of CMIP5 and the experiment
700 design, Bull. Amer. Meteor. Soc., 93 (4), 485-498, 2012.

701 Teuling, A. J., Hirschi, M., Ohmura, A., Wild, M., Reichstein, M., Ciais, P., Buchmann, N.,
702 Ammann, C., Montagnani, L., Richardson, A. D., Wohlfahrt, G., and Seneviratne, S. I.: A
703 regional perspective on trends in continental evaporation, Geophys. Res. Lett., 36,
704 L02404, doi:10.1029/2008GL036584, 2009.

705 Walsh, J. E., Anisimov, O., Hagen, J. O. M., Jakobsson, T., Oerlemans, J., Prowse, T. D.,
706 Romanovsky, V., Savelieva, N., Serreze, M., Shiklomanov, A., Shiklomanov, I.,
707 Solomon, S., Arendt, A., Atkinson, D., Demuth, M. N., Dowdeswell, J., Dyurgerov, M.,

Glazovsky, A., Koerner, R. M., Meier, M., Reeh, N., Sigurosson, O., Steffen, K., and Truffer, M.: Cryosphere and hydrology, in: Symon C, Arris L, Heal B (eds.) Arctic Climate Impact Assessment, Chap. 6: 184-242, Cambridge University Press, 2005.

Weedon, G. P., Balsamo, G., Bellouin, N., Gomes, S., Best, M. J., and Viterbo, P.: The WFDEI meteorological forcing data set: WATCH Forcing Data methodology applied to ERA-Interim reanalysis data, Water Resour. Res., 50, doi:10.1002/2014WR015638, 2014.

716 **Figure captions**

717 Fig. 1 Boreal summer (JJA) precipitation differences [%] relative to WFDEI data for a)
718 ECH6-REF, b) ECH6-PF, and c) difference between ECH6-PF and ECH6-REF [in
719 % of WFDEI precipitation].

720 Fig. 2 Boreal summer (JJA) 2m temperature differences [K] to WFDEI data for a) ECH6-
721 REF, b) ECH6-PF, and c) difference between ECH6-PF and ECH6-REF.

722 Fig. 3 Boreal summer (JJA) surface solar incoming radiation differences [W/m²] to CERES
723 data for a) ECH6-REF, b) ECH6-PF, and c) difference between ECH6-PF and
724 ECH6-REF.

725 Fig. 4 Catchments of the Baltic Sea and of the six largest Arctic rivers (from left to right:
726 Mackenzie, Baltic Sea, Northern Dvina, Ob, Yenisei, Lena, Kolyma).

727 Fig. 5 Mean monthly climatology (1989-2009) of discharge (upper panels) and
728 precipitation (lower panels) over the 6 largest Arctic river catchments (left column)
729 and the Baltic Sea catchment (land only, right column). Observations comprise
730 climatological observed discharge and WFDEI precipitation, respectively.

731 Fig. 6 Mean monthly climatology (1989-2009) of evapotranspiration (upper panels) and
732 relative root zone soil moisture (lower panels) over the 6 largest Arctic river
733 catchments (left column) and the Baltic Sea catchment (land only, right column).
734 Evapotranspiration data comprise the mean, minimum and maximum diagnostic
735 estimates from the LandFlux Eval (LF) dataset. The dashed blue line (PF-Total)
736 denotes the total root zone moisture content (liquid + frozen) for ECH6-PF.

737 Fig. 7 Mean frozen fraction of total root zone soil moisture (1989-2009) in ECH6-PF over
738 the 6 largest Arctic river catchments (solid curve) and the Baltic Sea catchment (land
739 only, dashed curve).

740 Fig. 8 Mean monthly climatological differences (1989-2009) between ECH6-PF and

741 ECH6-REF for precipitation (ΔP) and evapotranspiration (ΔET) over the 6 largest
742 Arctic rivers (upper panel) and the Baltic Sea catchment (lower panel). The dashed
743 lines indicate the corresponding spreads obtained from MPI-ESM simulations of
744 deVrese et al. (2016).
745 Fig. 9 Mean monthly climatology (1989-2009) of 2m temperature differences to WFDEI
746 data (upper panels) and surface solar irradiance (SSI; lower panels) over the 6 largest
747 Arctic river catchments (left column) and the Baltic Sea catchment (land only, right
748 column). SSI observations comprise CERES data for 2000-2010.
749 Fig. 10 Mean monthly climatology (1989-2009) of surface albedo (upper panels) and snow
750 pack snow water equivalent (SWE; lower panels) over the 6 largest Arctic river
751 catchments (left column) and the Baltic Sea catchment (land only, right column).
752 Albedo observations data from MODIS (2000-2011), CERES (2000-2010) and
753 GlobAlbedo (1998-2011), SWE observations comprise data from GlobSnow (1989-
754 2009), MERRA (1979-2013), and SDC climatology.
755 Fig. 11 Chain of processes involved in the soil moisture precipitation feedback over high
756 latitudes. Red arrows indicate the initiation of the positive feedback loop by the
757 presence of frozen soil, blue arrows indicate the loop itself.
758 Fig. 12 Correlation of soil moisture and precipitation for a) ECH6-REF, b) ECH6-PF, and c)
759 difference between ECH6-PF and ECH6-REF.
760 Fig. 13 Number of months where in the climatological average of 1989-2009, the upper soil
761 layer is below 0°C in ECH6-PF.
762

a)

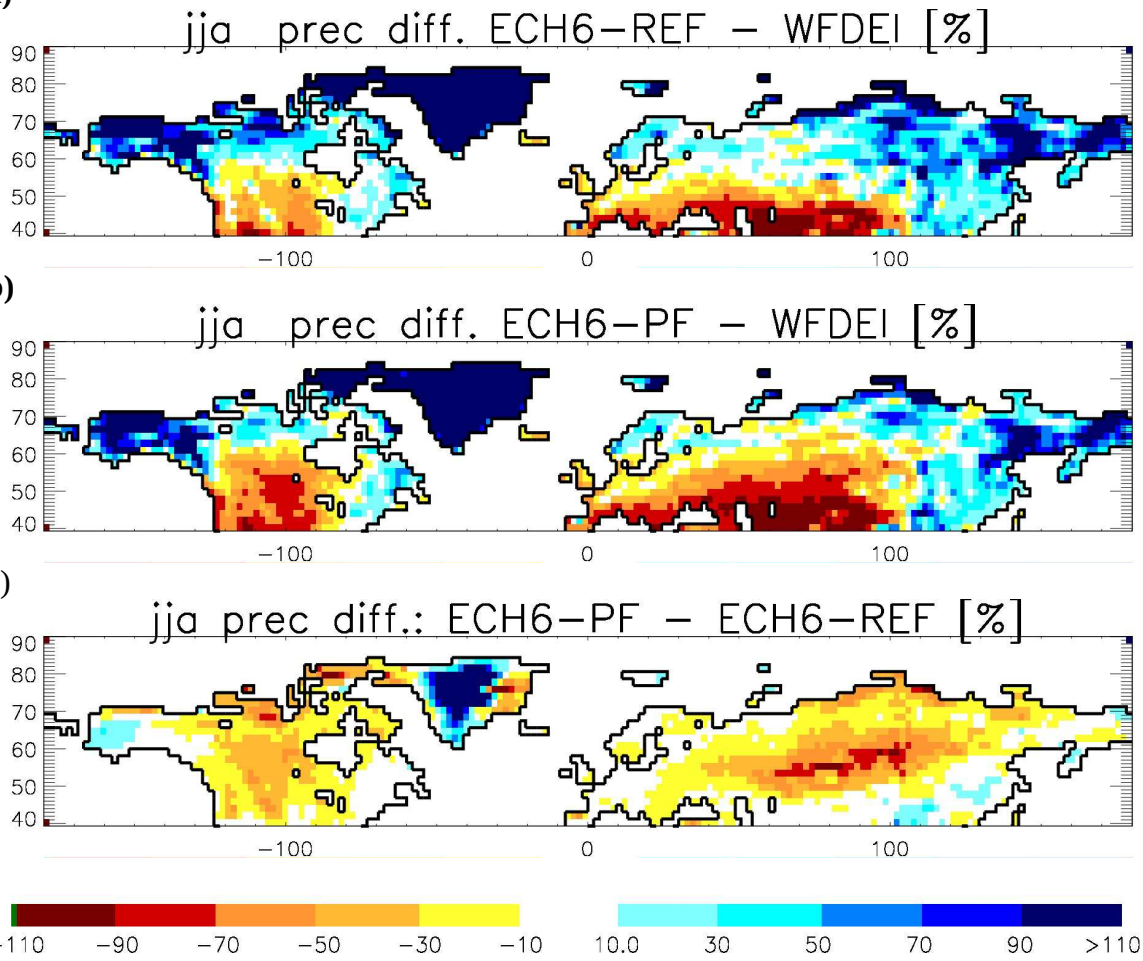

Fig. 1. Boreal summer (JJA) precipitation differences [%] relative to WFDEI data for a) ECH6-REF, b) ECH6-PF, and c) difference between ECH6-PF and ECH6-REF [in % of WFDEI precipitation].

a)

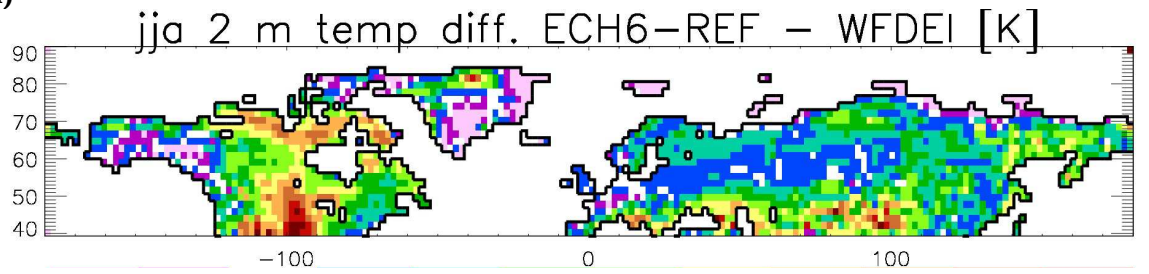

b)

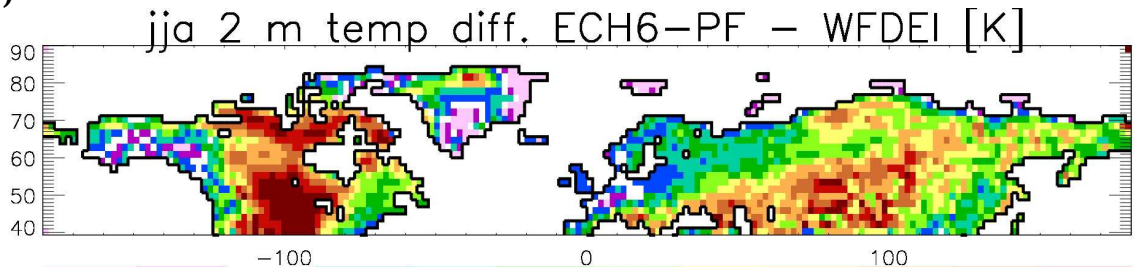

c)

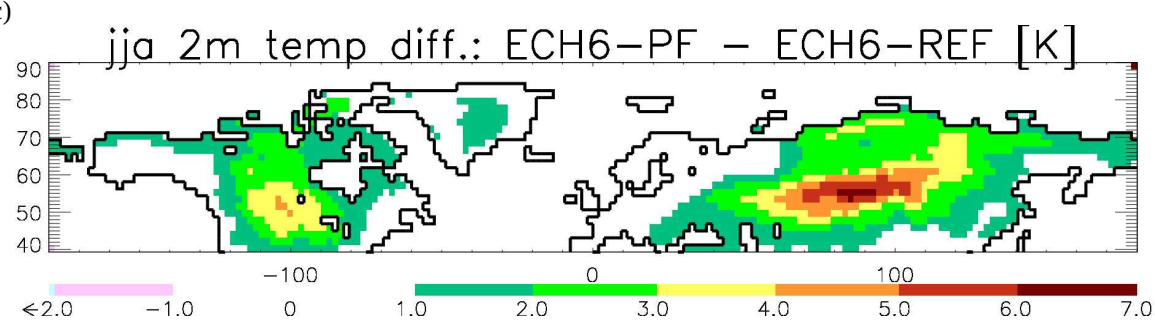

Fig. 2. Boreal summer (JJA) 2m temperature differences [K] to WFDEI data for a) ECH6-REF, b) ECH6-PF, and c) difference between ECH6-PF and ECH6-REF.

a)

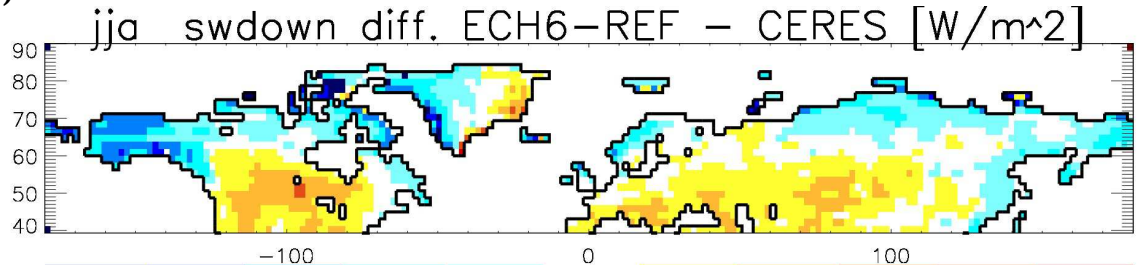

b)

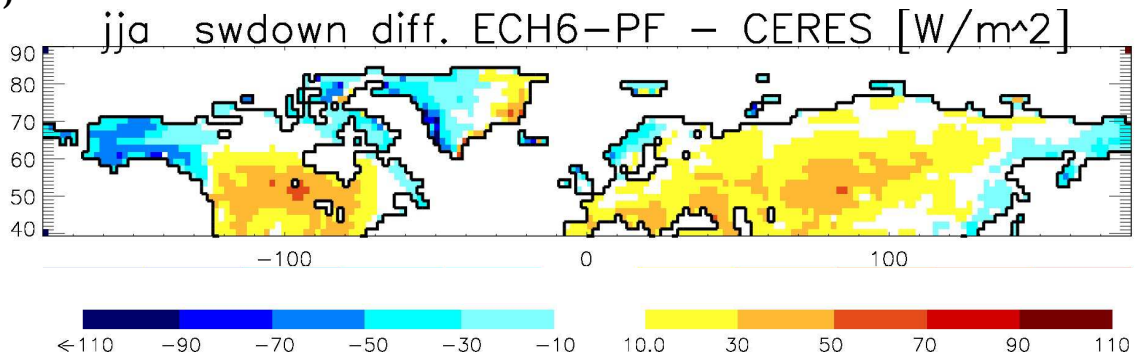

c)

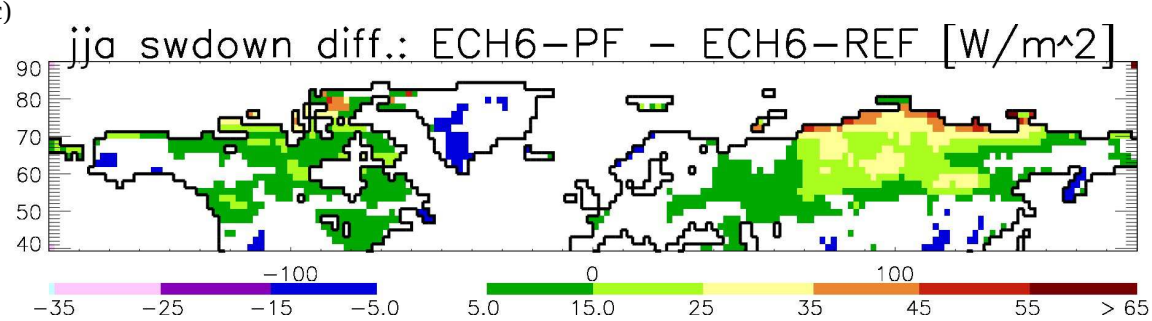

Fig. 3. Boreal summer (JJA) surface solar incoming radiation differences [W/m²] to CERES data for a) ECH6-REF, b) ECH6-PF, and c) difference between ECH6-PF and ECH6-REF.

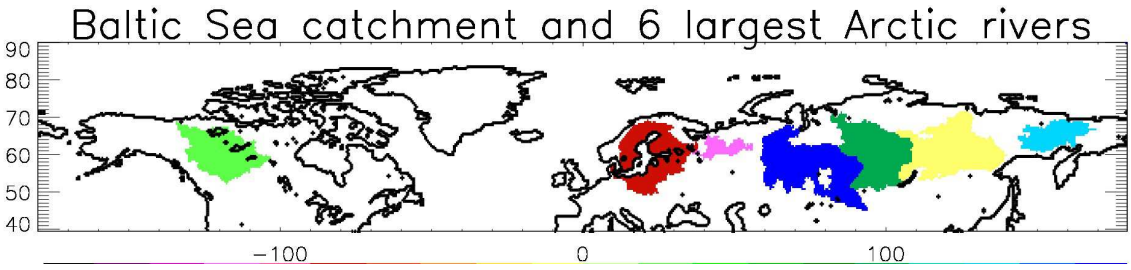

Fig. 4. Catchments of the Baltic Sea and of the six largest Arctic rivers (from left to right: Mackenzie, Baltic Sea, Northern Dvina, Ob, Yenisei, Lena, Kolyma).

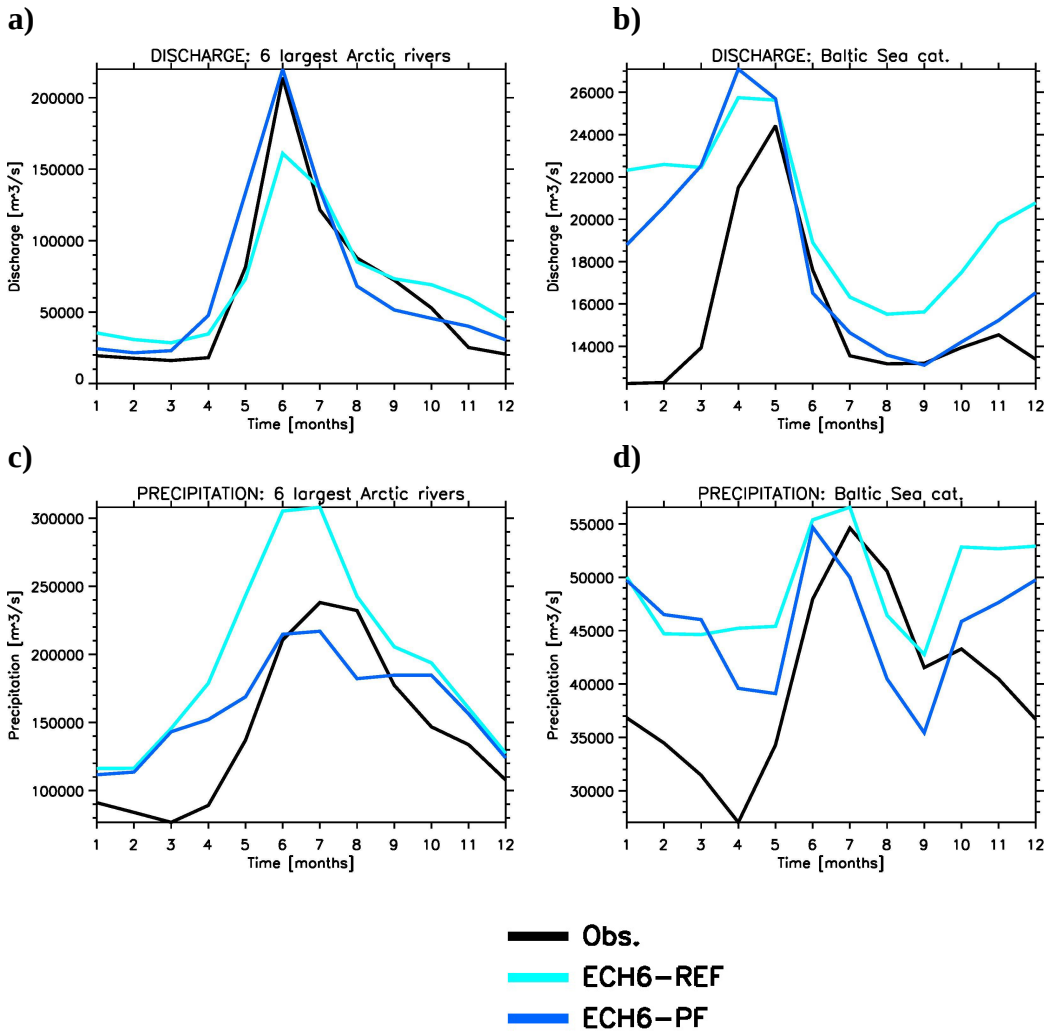

Fig. 5. Mean monthly climatology (1989-2009) of discharge (upper panels) and precipitation (lower panels) over the 6 largest Arctic river catchments (left column) and the Baltic Sea catchment (land only, right column). Observations comprise climatological observed discharge and WFDEI precipitation, respectively.

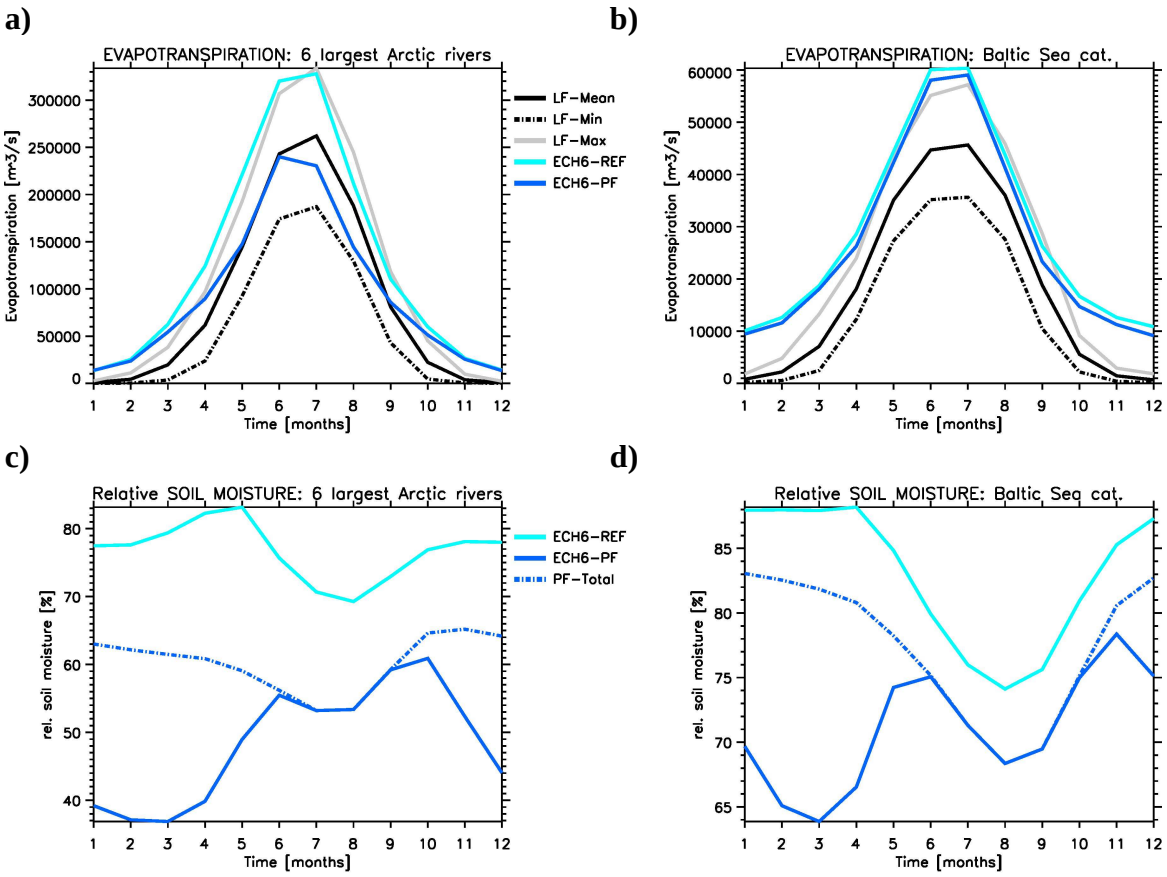

Fig. 6. Mean monthly climatology (1989-2009) of evapotranspiration (upper panels) and relative root zone soil moisture (lower panels) over the 6 largest Arctic river catchments (left column) and the Baltic Sea catchment (land only, right column). Evapotranspiration data comprise the mean, minimum and maximum diagnostic estimates from the LandFlux Eval (LF) dataset. The dashed blue line (PF-Total) denotes the total root zone moisture content (liquid + frozen) for ECH6-PF.

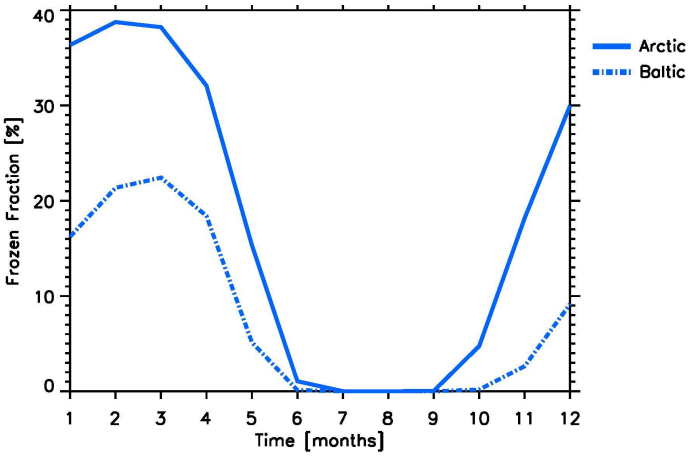

Fig. 7. Mean frozen fraction of total root zone soil moisture (1989-2009) in ECH6-PF over the 6 largest Arctic river catchments (solid curve) and the Baltic Sea catchment (land only, dashed curve). Note that for ECH6-REF, this is zero as no freezing is regarded.

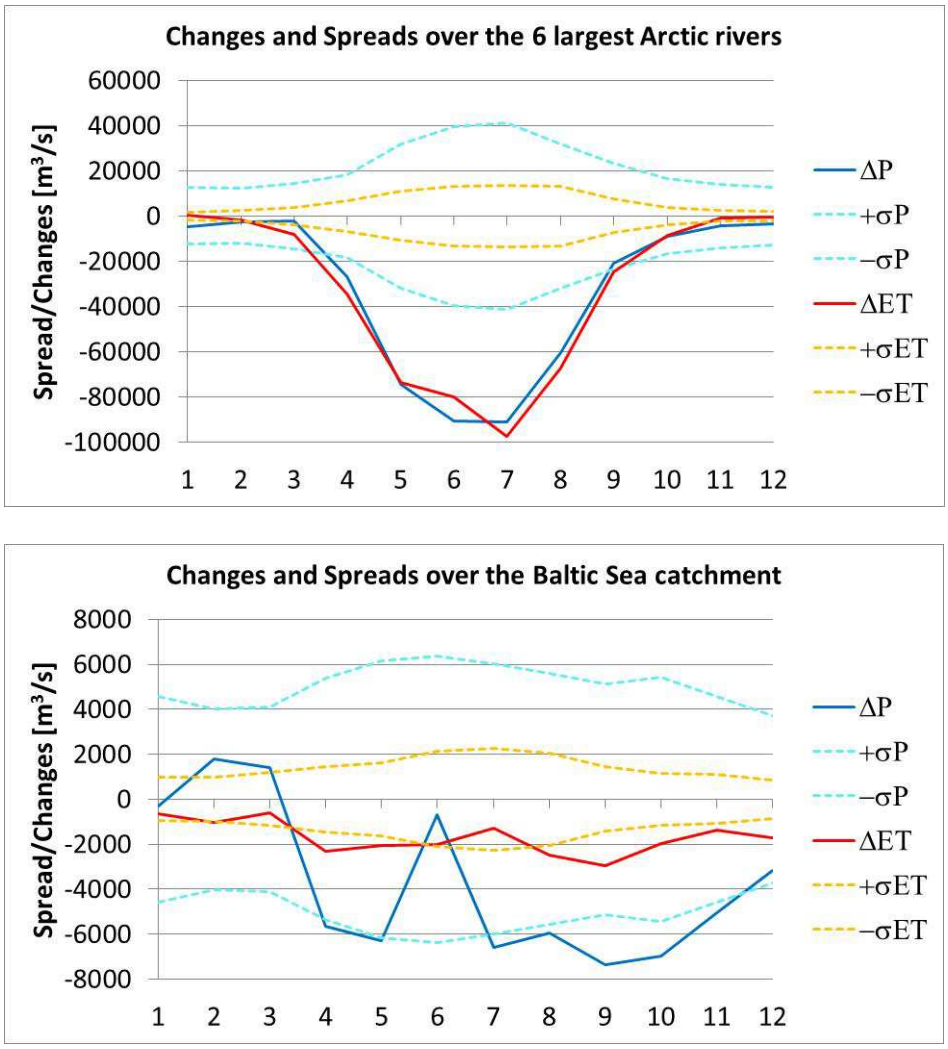

Fig. 8. Mean monthly climatological differences (1989-2009) between ECH6-PF and ECH6-REF for precipitation (*ΔP*) and evapotranspiration (*ΔET*) over the 6 largest Arctic rivers (upper panel) and the Baltic Sea catchment (lower panel). The dashed lines indicate the corresponding spreads obtained from MPI-ESM simulations of deVrese et al. (2016).

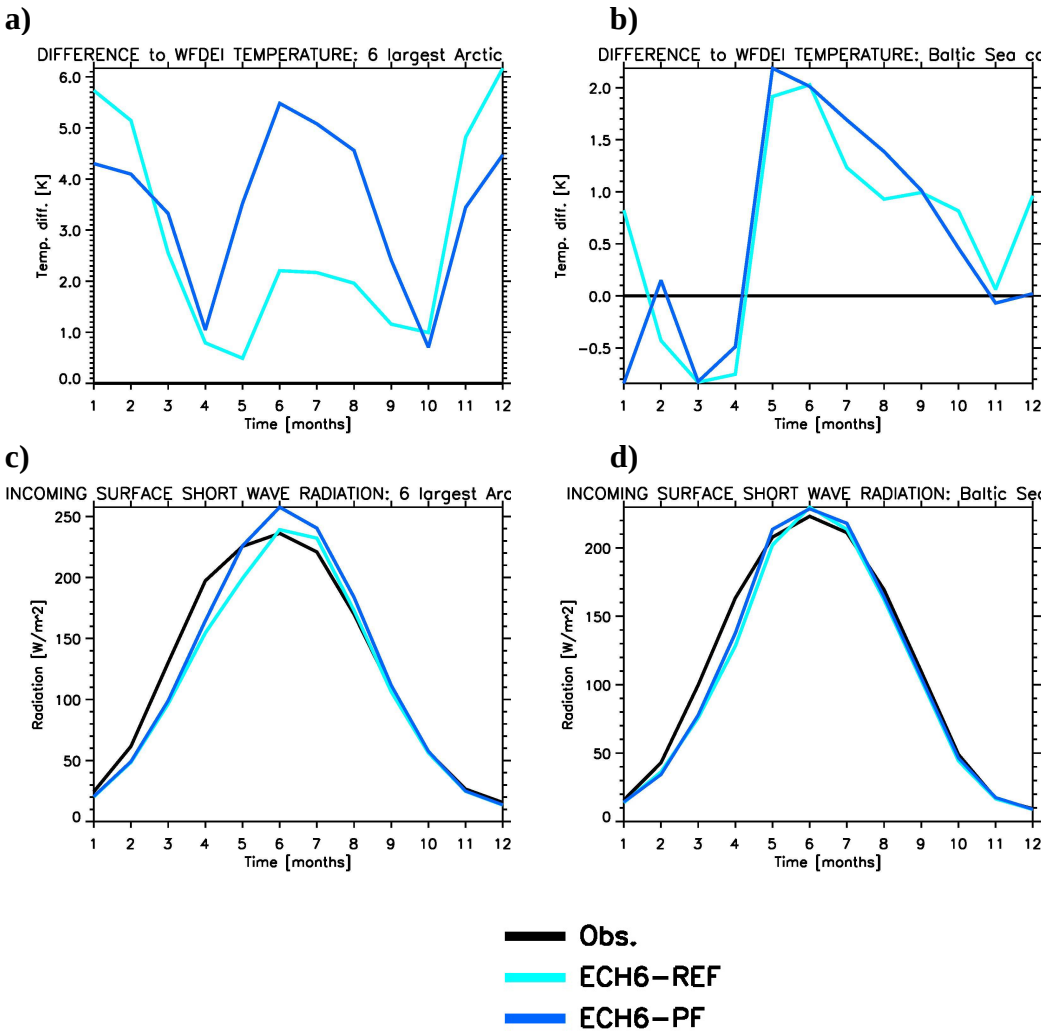

Fig. 9. Mean monthly climatology (1989-2009) of 2m temperature differences to WFDEI data (upper panels) and surface solar irradiance (SSI; lower panels) over the 6 largest Arctic river catchments (left column) and the Baltic Sea catchment (land only, right column). SSI observations comprise CERES data for 2000-2010.

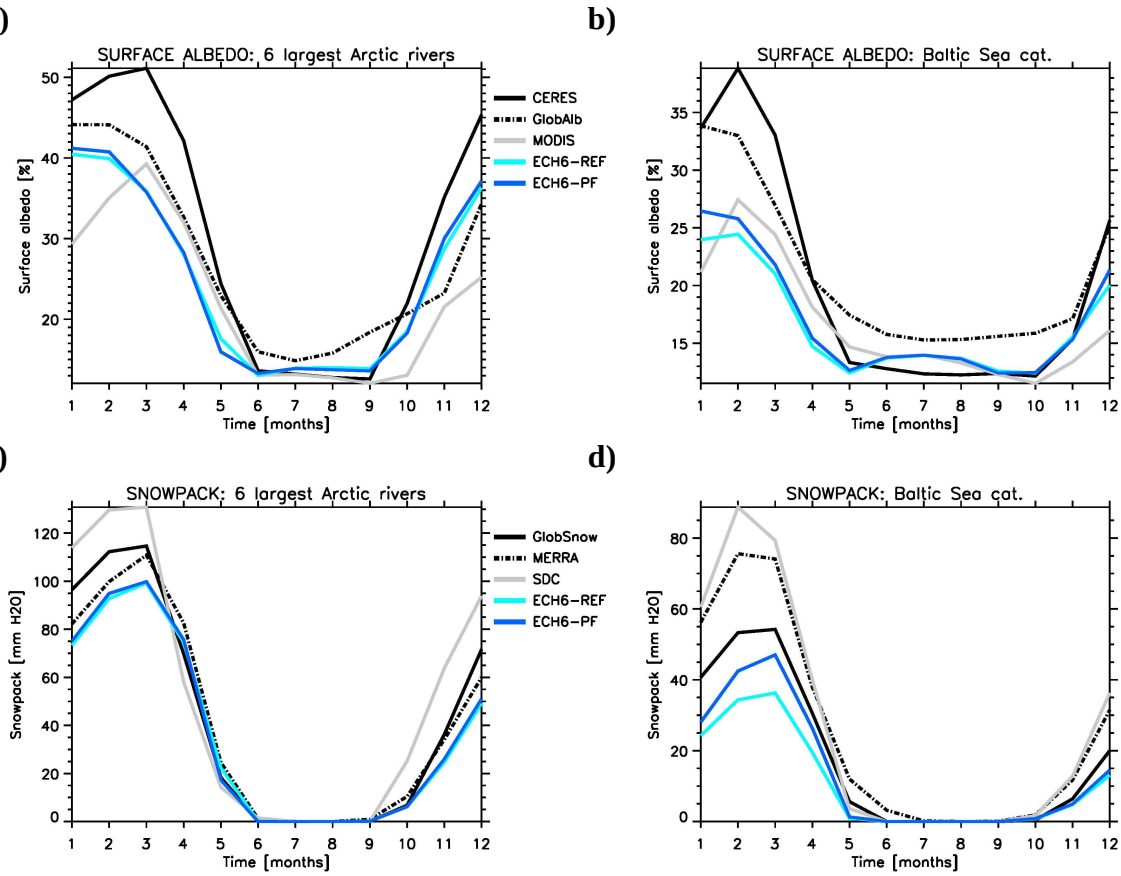

Fig. 10. Mean monthly climatology (1989-2009) of surface albedo (upper panels) and snow pack snow water equivalent (SWE; lower panels) over the 6 largest Arctic river catchments (left column) and the Baltic Sea catchment (land only, right column). Albedo observations data from MODIS (2000-2011), CERES (2000-2010) and GlobAlbedo (1998-2011), SWE observations comprise data from GlobSnow (1989-2009), MERRA (1979-2013), and SDC climatology.

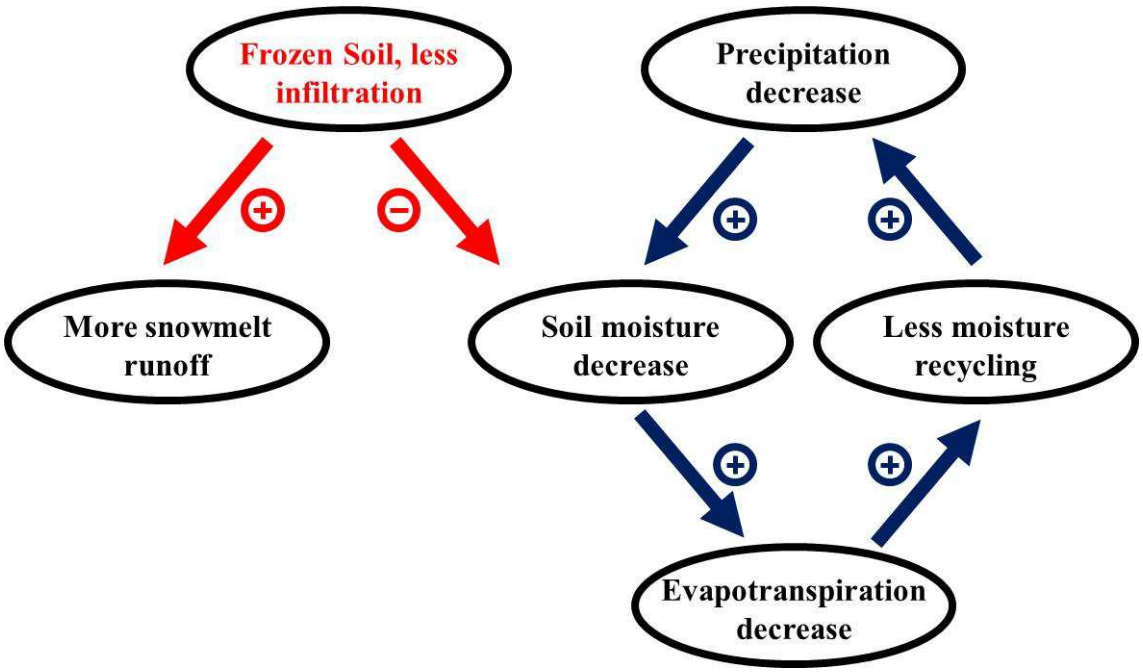

Fig. 11. Chain of processes involved in the soil moisture precipitation feedback over high latitudes. Red arrows indicate the initiation of the positive feedback loop by the presence of frozen soil, blue arrows indicate the loop itself.

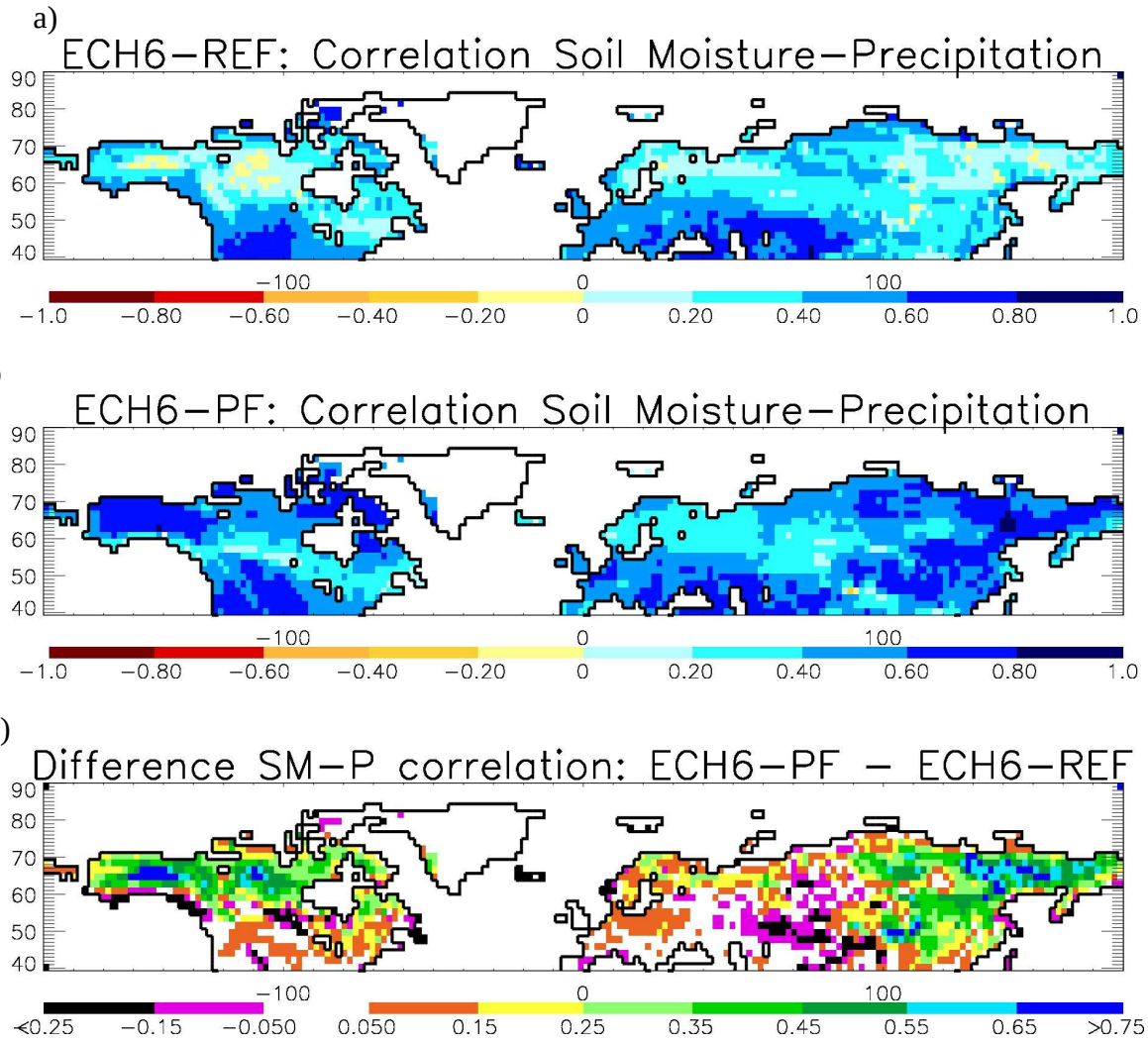

Fig. 12. Correlation of soil moisture and precipitation for a) ECH6-REF, b) ECH6-PF, and c) difference between ECH6-PF and ECH6-REF.

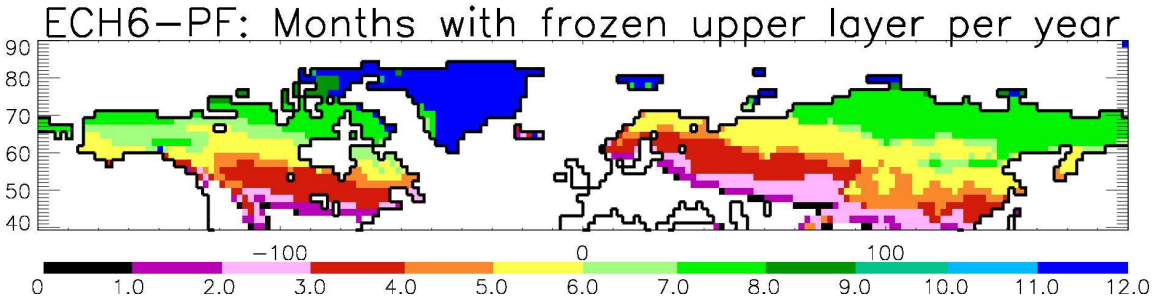

Fig. 13. Number of months where in the climatological average of 1989-2009, the upper soil layer is below 0°C in ECH6-PF.

906 **Table 1.** Summer (JJA) biases over the six largest Arctic rivers for 2m temperature (T_{2m}, to
907 WFDEI), radiative flux (R) into the surface due to biases in SSI (to CERES), albedo (α, to
908 GlobAlbedo) and their combined effect (comb.) as well as the estimated related impact on
909 surface temperature (T_s) and the contribution of the SSI bias to this impact.

Experiment	ΔT_{2m}	ΔR SSI	ΔR α	ΔR comb.	ΔT_s comb.	SSI cont.
ECH6-REF	2.1 K	5.0 W/m²	4.1 W/m²	9.0 W/m²	1.7 K	55%
ECH6-PF	5.0 K	15.8 W/m²	4.3 W/m²	19.8 W/m²	3.6 K	78%

910

911